Imaging Net Retrograde Axonal Transport In Vivo: A Physiological Biomarker

Pin-Tsun Justin Lee, BS [1†] Zachary Kennedy, PhD,[1,2†] Yuzhen Wang, PhD,[3] Yimeng Lu, PhD,[4] Carolina Cefaliello, PhD [1] Özgün Uyan, MS,[1] Chun-Qing Song, PhD,[2,5] Bruno Miguel da Cruz Godinho, PhD,[2,5] Zuoshang Xu, PhD,[6] Mary Rusckowski, PhD,[3] Wen Xue, PhD,[2,5] and Robert H. Brown Jr MD, DPhil [1]

Objective: The objective of this study is to develop a novel method for monitoring the integrity of motor neurons in vivo by quantifying net retrograde axonal transport.
Methods: The method uses single photon emission computed tomography to quantify retrograde transport to spinal cord of tetanus toxin fragment C (^{125}I-TTC) following intramuscular injection. We characterized the transport profiles in 3 transgenic mouse models carrying amyotrophic lateral sclerosis (ALS)-associated genes, aging mice, and SOD1^{G93A} transgenic mice following CRISPR/Cas9 gene editing. Lastly, we studied the effect of prior immunization of tetanus toxoid on the transport profile of TTC.
Results: This technique defines a quantitative profile of net retrograde axonal transport of TTC in living mice. The profile is distinctly abnormal in transgenic SOD1^{G93A} mice as young as 65 days (presymptomatic) and worsens with disease progression. Moreover, this method detects a distinct therapeutic benefit of gene editing in transgenic SOD1^{G93A} mice well before other clinical parameters (eg, grip strength) show improvement. Symptomatic transgenic PFN1$^{C71G/C71G}$ ALS mice display gross reductions in net retrograde axonal transport, which is also disturbed in asymptomatic mice harboring a human *C9ORF72* transgene with an expanded GGGGCC repeat motif. In wild-type mice, net retrograde axonal transport declines with aging. Lastly, prior immunization with tetanus toxoid does not preclude use of this assay.
Interpretation: This assay of net retrograde axonal transport has broad potential clinical applications and should be particularly valuable as a physiological biomarker that permits early detection of benefit from potential therapies for motor neuron diseases.

ANN NEUROL 2022;91:716–729

Axonal transport is an essential cellular process required for proper maintenance of health and function in neurons. The bidirectional communication between cell body and its distal axon terminals, which in human spinal motor neurons can extend to a meter in length, depends on functional axonal transport. This continuous transport includes anterograde movement of cytoskeletal elements, mitochondria, newly synthesized proteins, RNAs, and lipids for maintenance of neuronal morphology and function, and retrograde movement of damaged, aged organelles and proteins for degradation and growth or injury signals from the environment.

View this article online at wileyonlinelibrary.com. DOI: 10.1002/ana.26329

Received Nov 24, 2021, and in revised form Feb 6, 2022. Accepted for publication Feb 14, 2022.

Address correspondence to Dr Brown, Department of Neurology, University of Massachusetts Medical School, 55 Lake Avenue North, Worcester, MA 01655. E-mail: robert.brown@umassmed.edu

[†]P.-T.J.L. and Z.K. contributed equally to this work.

From the [1]Department of Neurology, University of Massachusetts Chan Medical School, Worcester, MA, USA; [2]RNA Therapeutics Institute, University of Massachusetts Chan Medical School, Worcester, MA, USA; [3]Department of Radiology, University of Massachusetts Chan Medical School, Worcester, MA, USA; [4]VIR Biotechnology, San Francisco, CA, USA; [5]Program in Molecular Medicine, Department of Molecular, Cell, and Cancer Biology, and Li Weibo Institute for Rare Disease Research, University of Massachusetts Chan Medical School, Worcester, MA, USA; and [6]Department of Biochemistry and Molecular Pharmacology, University of Massachusetts Chan Medical School, Worcester, MA, USA

Additional supporting information can be found in the online version of this article.

Alterations in axonal transport have emerged as a common theme in a variety of neurodegenerative disorders, such as Alzheimer disease, Parkinson disease, and amyotrophic lateral sclerosis (ALS), and in normal aging.[1] Several lines of investigation incriminate deficits in anterograde and retrograde axonal transport in ALS. Cargo protein aggregation and changes in transport speed and frequency of various cargoes transported in both directions are well documented in ALS patients and transgenic animal models, occurring months before other signs of neurodegeneration.[2-15] Genetic studies have identified associations between multiple genes involved in axonal transport and ALS, including *KIFAP3, PFN1, TUBA4A, NEK1*, and dynactin.[16-19] By activating p38 mitogen and inhibiting kinesin 1, mutations in the ALS gene *SOD1* perturb the dynactin–dynein complex ratio and inhibit retrograde transport.[7,20,21] Multiple pathophysiological features likely contribute to the deficiencies of axonal transport in ALS, potentially including mitochondrial dysfunction, disturbances in RNA metabolism, protein instability,[22]and the accumulation of aggregated proteins such as TDP43 in the axon.[23] It is also possible that noncell autonomous factors disturb axonal function, involving microglia, astrocytes, or interneurons. Given the diversity of ALS pathologies, the pathophysiology of axonal transport may well differ in sporadic versus familial ALS, or even within different genetic forms of familial ALS.

We report here an in vivo method to image quantitatively and repeatedly retrograde transport from muscle to motor neurons of a nontoxic tetanus toxin designated TTC. This uptake reflects the activity of the retrograde axonal transport machinery and the integrity of the neuromuscular junctions (NMJs), as well as the total number of viable motor neurons. We therefore define this as "net retrograde axonal transport." This technique will be useful not only in studying axonal transport dynamics but also as an imaging biomarker to detect early benefit from effective therapies and to measure overall motor neuron health in disease and aging processes.

Materials and Methods

Recombinant Expression, Purification, and Radiolabeling of TTC

Recombinant TTC (residues 865–1,315 of TTC) was purified as described.[24] Radiolabeled TTC was prepared by incubating 30μg of TTC per mCi of ^{125}I-radionuclide (PerkinElmer, Waltham, MA) using the Iodogen reaction. After 10 minutes of incubation, tyrosine was added to quench the reaction, and the sample was then purified by P-6 spin column (Bio-Rad Laboratories, Hercules, CA) into phosphate-buffered saline (PBS).

Evaluation of ^{125}I-TTC Affinity to Its Binding Sites on Mammalian Membrane

To determine binding affinity of radiolabeled TTC to its receptors in synaptosomes, we used a TTC displacement assay.[25]

Animals

Animal studies were approved by the institutional animal care and use committee at the University of Massachusetts Chan Medical School. Transgenic mice carrying a human *SOD1* mutant gene (B6SJL-Tg[SOD1-G93A]1Gur/J), and wild-type C57BL6 and FVB/NJ mice were from Jackson Laboratory (Bar Harbor, ME). Thy1.2-PFN1$^{C71G/C71G}$ transgenic mice were prepared by Dr Zuoshang Xu[26]; the *C9ORF72* transgenic (C9BAC) mice were produced in our laboratory.[27]

Single Photon Emission Computed Tomographic/Computed Tomographic Imaging

One week prior to imaging, animals were pretreated with potassium iodide to block thyroid uptake of free ^{125}I. Approximately 10μg of radiolabeled TTC was injected into the lateral gastrocnemius muscle in the anesthetized animals. All animals were imaged at multiple time points over 2 weeks to monitor transport of TTC using a NanoSPECT/CT camera (BioScan, Geneva, Switzerland). Standard resolution with 45kVp voltage and 500-millisecond exposure time was used to perform computed tomographic (CT) scanning; the parameters of the single photon emission CT (SPECT) imaging were 1.0mm/pixel, 256 × 256 frame size, and 60 seconds per projection for a total of 24 projections. Animals were imaged under anesthesia. The completed CT and SPECT images were reconstructed, and the volume-of-interest (VOI) analysis of the SPECT acquisitions was carried out by VivoQuant 1.23 software (InviCRO, Boston, MA). At each time point, we subtracted from uptake in the designated VOI the background uptake of ^{125}I-TTC in an equivalent but remote VOI; this yielded the uptake specific to the region of interest in the anterior gray matter of the spinal cord. The radioactivity of VOI in each animal was normalized to that of its wild-type and age-matched controls; in the aging study, VOI radioactivity was normalized to that of young (50-day-old) mice. For the sciatic nerve-dependent study, 85-day-old male C57BL6 mice without (n = 4) or with (n = 6) transection of the sciatic nerve were used. For the SOD1^{G93A} ALS study, 45- (n = 5), 65- (n = 5), 85- (n = 6), 110- (n = 9), and 125-day-old (n = 5) male B6SJL-Tg[SOD1-G93A]1Gur/J mice were used, along with their age-matched littermates (n = 30). For the CRISPR-Cas9 treatment study, 85-day-old female SOD1^{G93A} mice with sgSOD1 treatment (n = 7), SOD1^{G93A} mice with sgControl treatment (n = 8), and age-matched nontransgenic control (nTg; n = 6) were used. For the C9BAC study, 700-day-old female C9BAC (n = 10) and age-matched nTg (n = 6) were used. For the aging study, 50- (n = 9), 100- (n = 11), 300- (n = 13), 500- (n = 14), 700- (n = 12), and 900-day-old (n = 5) C57BL6 male mice were used. For the immunization study, nonimmunized (n = 13), immunized plus 1 booster (n = 10), and immunized plus 2 boosters (n = 8) C57BL6 mice were used.

TABLE. CRISPR Cas9 Oligonucleotide Sequences

Notes	ID	Sequence (5′ to 3′) or Plasmid Name
sgSOD1 sequence	1657 sghSOD1.E2c	CACCGAATGGACCAGTGAA GGTGTG
sgControl sequence[a]	sgLacZ (Addgene 60228)	TGCGAATACGCCCACGCGAT
SOD1 genotyping primer	mSOD fwd	GCATACCCAATCACTCCACAG
SOD1 genotyping primer	mSOD rev	GTCCATGAGAAACAAGATGAC
SOD1 genotyping primer	hSOD fwd	CATCAGCCCTAATCCATCTGA
SOD1 genotyping primer	hSOD rev	TCTTAGAAACCGCGACTAACAATC
Sequencing library primer	1811 SOD1exon2.F	CCATCTCCCTTTTGAGGACA
Sequencing library primer	1812 SOD1exon2.R	CGACAGAGCAAGACCCTTTC
Backbone AAV-sgRNA	Addgene 60228	AAV:ITR-U6-sgRNA(LacZ)-pCBh-Cre-WPRE-hGHpA-ITR
Backbone AAV-sgRNA	Addgene 60958	pAAV-U6sgRNA_hSyn-GFP-KASH-bGH
Backbone-AAV Cas9	AAV.Cas9	pAAV-pU1A-spCas9-RBGpA Cas9
Backbone-Lenti sgRNA/Cas9	Addgene 52961	lentiCRISPR v2

[a]Initially published in Platt et al.[28]

CRISPR-Cas9-Mediated Knockdown of SOD1

We designed single-guide RNAs (sgRNAs) targeting human *SOD1* using the CRISPR design tool (crispr.mit.edu; Table). Oligonucleotides encoding the sgRNA sequences were synthesized (Genewiz, South Plainfield, NJ). For in vitro screening, we used lentiCRISPRv2 Cas9-FLAG-2A-Puro (Addgene, Cambridge, MA) to generate stable HCT116 cell lines (human diploid colorectal cells) expressing Cas9 and our sgRNA. For delivery of sgRNA to mice, plasmid pAAV-U6-sgRNA (Addgene) and plasmid hSyn-GFP-KASH-bGH (a kind gift of Dr Feng Zhang, Massachusetts Institute of Technology), were packaged into AAV9 vectors using the UMass Vector Core.

AAV9.Cas9 and AAV9.guide vectors were coinjected into the lateral cerebral ventricles of postnatal day 1 B6SJL-Tg (SOD1-G93A)1Gur/J[29] (8E9 genome copies/μl for the AAV9.cas9 vector; 9E9 genome copies/μl for the AAV9.guide vector) mice (n = 39). Control groups included untreated $SOD1^{G93A}$ mice (n = 13), $SOD1^{G93A}$ mice treated only with AAV9.Cas9 (n = 4), and $SOD1^{G93A}$ mice treated with AAV9.Cas9 and an AVV9 expressing a nontargeting guide RNA (sgControl; n = 13). Mice were observed weekly for signs of paresis/paralysis and sacrificed at disease endpoint, defined by the inability of a mouse to right itself within 10 seconds after being placed on its back. To measure human SOD1 protein, tissues were homogenized in radioimmunoprecipitation assay buffer with a protein inhibitor cocktail (Roche, Basel, Switzerland) and assayed via enzyme-linked immunosorbent assays (ELISAs; Invitrogen, Carlsbad, CA).

Immunohistochemistry

All spinal cord tissues were sectioned using a cryostat, blocked with 0.4% Triton X-100, 4% donkey serum, and 4% bovine serum albumin (Sigma-Aldrich, St Louis, MO) in PBS, and incubated with polyclonal antibodies against TTC (Rockland, Gilbertsville, PA), and IBA1 (Novus Biologicals, Littleton, CO), or monoclonal antibodies against ALDH1L1 (Millipore, Billerica, MA), and GAD67 (Abcam, Cambridge, MA). Thereafter, sections were incubated with Alexa Fluor 488 antirabbit secondary antibody (Abcam) and Alexa Fluor 594 antimouse secondary antibody (Invitrogen) and mounted in ProLong Diamond Antifade Mountant with 4,6-diamidino-2-phenylindole (Life Technologies, Carlsbad, CA). Images were acquired using a TissueFAXS iQ tissue cytometer (TissueGnostics, Studio City, CA), captured with an Orca Fusion BT camera (Hamamatsu Photonics, Hamamatsu, Japan), and analyzed with the TissueFAXS Viewer software. NMJ staining was performed as described previously[27]; a blinded observer scored each NMJ as either intact, partially denervated, or fully denervated. Mice from the following groups were compared: untreated, Cas9 + sgSOD1, and Cas9 + sgControl (n = 3 mice for each group).

Laser Capture Microdissection and Gel Capillary Western Blot of Motor Neurons

All laser capture microdissection was performed using the Arcturus (Mountain View, CA) XT laser capture system.[30] Frozen, unfixed spinal cord tissue embedded in optimal cutting temperature medium were cut into 10μm sections using a cryostat and

stored at −80°C. Lysates were analyzed using the ProteinSimple (San Jose, CA) Wes capillary Western blot machine using an SOD1 antibody (R&D Systems, Minneapolis, MN) and normalized to total protein levels using the ProteinSimple Total Protein Labeling kit (ProteinSimple). Results were analyzed using Compass SW software (v4.4.0, ProteinSimple).

Tetanus Toxoid Vaccination and Tetanus Antibody Titer Assay

For immunization against tetanus, C57BL6 male mice received tetanus toxoid (TT) in the gastrocnemius muscle (MassBiologics, UMass Chan Medical School, Boston, MA; 90 flocculation units, 10μl) at 8 weeks of age and a follow-up booster 6 weeks later in the same muscle (n = 12). For the naïve/control animals, PBS was administered instead of TT (n = 12). Six weeks after the booster shot, ^{125}I-TTC was administered intramuscularly (10μg) into both immune and naïve mice for the net retrograde axonal transport assay. To study the effect of immunization against TTC on net retrograde axonal transport, a second dose of ^{125}I-TTC was administered 10 weeks after the initial net axonal transport assay. Mouse IgG antibody against TT was measured by ELISA (XpressBio, Frederick, MD). Mouse sera were collected prior to 4 key time points: the primary TT injection, the TT booster, and the first and second TTC uptake assays.

Statistical Analysis

For analysis of different experimental groups of transport profiles, comparisons were based on a mixed model for repeated measures. The model included all measurements (excluding the first 2 time points: time at 0 hours and time at 30 minutes) as the dependent variable; experiment group, visit, and treatment-by-visit interaction as the fixed effects; and individual mice as a random effect. A compound symmetry covariance structure was used to model the within-subject errors. With a mixed-effects model based on restricted maximum likelihood estimation used for the analysis, no imputation of missing data was performed, assuming data were missing at random, conditional on the fixed and random effects. The primary result obtained from the model was the least-squares mean differences between the experimental groups from 24-hour time points through the last time points. The least-squares mean differences along with the corresponding 95% confidence intervals, and the 2-sided p values were provided. The least-squares means for each treatment group, as well as the corresponding 95% confidence intervals were provided as well (Table S1).

For survival analysis of CRISPR-Cas9-treated mice, differences in Kaplan–Meier curves were determined by log-rank test. For ELISA, grip strength, NMJ, and ventral horn analyses, Student t tests were used to compare sgSOD1 mice and control cohorts. GraphPad Software (San Diego, CA) Prism 8 or Microsoft (Redmond, WA) Excel was used to compute statistical analysis.

Statistically significance inferences of immunohistochemical TTC colabeling in the anterior horn of the spinal cord were reported as fold change of pixel colocalization over time. ImageJ's JACoP script was used to compute Mander's Overlap Coefficient, which is a ratio of number of pixels containing both TTC and cell marker signal to the total number of pixels containing cell marker signal. To correct for background noise, fold change was normalized to pixel colocalization of negative control images, that is, images of the anterior horn that contained no TTC signal. Statistical significance of changes in colocalization over time was determined using a mixed effects model corrected with Tukey multiple comparison test. GraphPad Prism 8 was used to compute statistical analysis.

Results

^{125}I-TTC Retains Cell Binding and Retrograde Transport Activity In Vivo

It is well established that TTC associates with ganglioside GT_{1b}, a surface binding partner.[31] To verify that iodination does not alter the specificity of binding of TTC to its receptors, we compared binding of native TTC and ^{127}I-TTC to N18-RE-105 cells, which express ganglioside GT_{1b}. Iodinated and native TTC showed comparable binding (Fig 1A). Neither ligand bound to HeLa cells and COS7 cells, which lack surface GT_{1b} (data not shown). We also assessed binding by TTC and radiolabeled ^{125}I-TTC to synaptosomes from mouse brain. The dissociation constant of ^{125}I-TTC (K_d approximately 100nM) was similar to that of TTC and reported values (see Fig 1B).[32] Thus, TTC and ^{125}I-TTC bind specifically and with equivalent affinity to cells and tissue expressing the tetanus receptor gangliosides.

We next studied the net retrograde axonal transport profile of ^{125}I-TTC following injection into limb muscles. We injected ^{125}I-TTC into the gastrocnemius muscle of healthy 85-day-old C57BL6 mice. Uptake into the L4–5 motor neurons ipsilateral to the injection was documented by repeatedly imaging each animal, initially at approximately every 6 hours, then every 24 hours up to two weeks (336 hours). For the first several hours, ^{125}I-TTC was detected diffusely in the chest and abdomen, reflecting distribution of TTC via the circulation; this diffuse signal cleared by 24 hours. In the ipsilateral L4–5 region (Video VIDEO S1), a distinct signal was evident at 24 hours, peaking at 48 hours postinjection and then slowly declining (Fig 1C). At 2 weeks postinjection, the signal was still evident, representing a decline of 70% of the peak. To verify that this signal was dependent on the integrity of retrograde transport of TTC within the sciatic nerve, we repeated this study in animals in which a fragment of the sciatic nerve had been resected 3 days prior to injection. No uptake of radioactivity was detected in the sciatic nerve resected mice (see Fig 1C, $p < 0.0001$, Table S1). These data demonstrate that ^{125}I-TTC is a reliable reagent for visualizing net retrograde axonal transport in vivo.

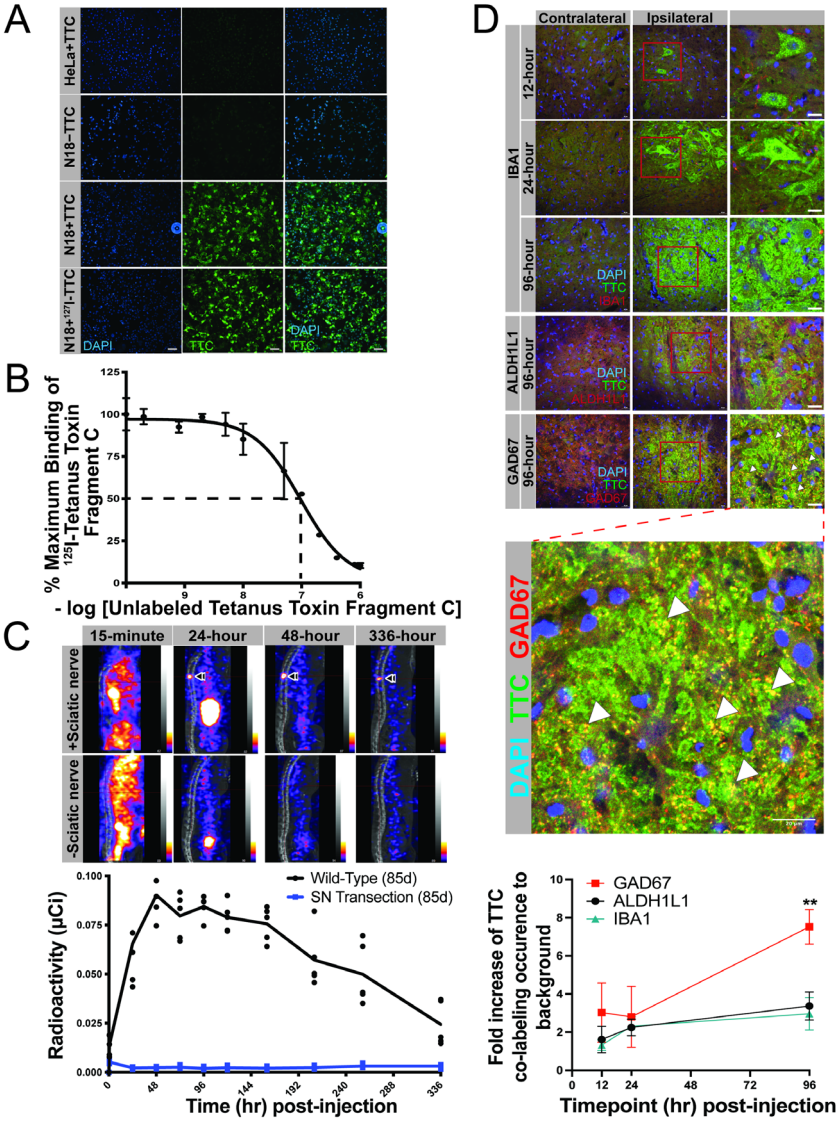

FIGURE 1: Iodination of tetanus toxin fragment C (TTC) does not impair receptor binding and permits quantification of net retrograde axonal transport. (A) Staining of TTC after incubating either native TTC or cold-iodinated TTC (^{127}I-TTC) with HeLa or N18-RE-105 (N18) cells documents that (1) binding of TTC is selective for cells that express the TTC-binding ganglioside GT_{1b} (N18-RE-105 but not HeLa), and (2) binding of TTC to the cell surface was not eliminated by iodination. (B) Radiolabeled TTC (^{125}I-TTC) binds with high affinity to its binding sites on mouse brain synaptosomes. The concentration of unlabeled TTC that displaces 50% of the maximum binding of ^{125}I-TTC is ~100nM. Each incubation of unlabeled TTC, labeled TTC, and synaptosomal preparations was done in quintuples. Error bars represent standard error of the mean. (C) The upper panel shows sagittal single photon emission computed tomographic/computed tomographic images of the thoracolumbar region of 85-day-old C57BL6 mice without (top row) and with (bottom row) transection of the sciatic nerve (SN). Arrowheads point to the accumulated ^{125}I-TTC at L4–5 lumbar segments. The graph in the bottom panel of C plots the quantitative uptake of TTC in the L4–5 region over time. Uptake is expressed as radioactivity in µCi and represents net retrograde axonal transport (n = 4 in the sciatic nerve-intact group, and n = 6 in the sciatic nerve-transected group). Data are presented as least-squares mean absolute radioactivity from time points from 24 to 336 hours (14 days) based on the mixed model for repeated measures, along with individual mouse data points. Least-squares mean differences ± standard errors (95% confident interval) were 0.072 ± 0.01 (0.05–0.09) with $p < 0.0001$ (see Table S1). (D) Immunohistochemistry shows TTC colocalization with GAD67^{+} γ-aminobutyric acidergic interneurons as the former emerges from the motor neurons as early as 24 hours postinjection (indicated by *arrowheads*), whereas no pronounced colocalizations of TTC and ALDH1L1-expressing astrocytes or IBA1-expressing microglia are observed at any of the time points. Bar = 20µm. DAPI = 4,6-diamidino-2-phenylindole.

Immunostaining the corresponding lumbar regions at 12, 24, and 96 hours after TTC administration confirmed the localization of TTC within the motor neurons in the anterior horns. Additionally, staining of TTC outlined the sensory neurons in the dorsal root ganglia at the same ipsilateral level of the spinal columns (data not shown). This reaffirms previous reports that TTC is taken up by both motor and sensory neurons.[33]

We examined the colocalization of TTC with various cell types in the spinal cord by double-labeling sections with TTC and either ALDH1L1 (astrocytes), IBA1 (microglia), or GAD67 (γ-aminobutyric acidergic [GABAergic] interneurons synaptic boutons).[34] We quantified the fold change of the ratio of colocalized pixels to total cell signal pixels, normalized to non-TTC-containing tissue. At 12 hours, the staining pattern of TTC was punctate and almost exclusively within motor neuron cell bodies, suggesting that most TTC resided in cytoplasmic vesicles within the motor neurons (see Fig 1D, upper panels). At 24 hours, some colocalization events were evident between TTC and GAD67 (indicated by arrowheads), but colocalization with TTC and any cell marker was not significant. At 96 hours after TTC administration, a robust and statistically significant increase in colocalization of TTC and GAD67 was observed (compared to 12 hours, $p < 0.01$, see Fig 1D, bottom panel). We did not see costaining of TTC and astrocytes (ALDH1L1-positive cells). Together, our observations are consistent with previous findings that TTC is retrogradely transported into spinal cord motor neurons[35] and translocates to motor neuron–interneuron synapses.[36]

Net Retrograde Axonal Transport Is Deficient in Transgenic SOD1^{G93A} ALS Mice

The transgenic ALS SOD1^{G93A} mouse displays deficiencies in retrograde axonal transport as early as 1 month prior to the onset of muscle denervation.[9] We recorded uptake of ^{125}I-TTC from the gastrocnemius muscle of SOD1^{G93A} mice at different disease stages: presymptomatic (45 and 65 days old), minimally symptomatic (85 days old), late symptomatic (110 days old), and terminal stages (125 days or older). Following intramuscular injection, the animals were imaged at 24- or 48-hour intervals in a 2-week span, and the radioactivity at corresponding L4–5 lumbar regions was quantified (Fig 2). Age-matched nontransgenic littermates served as controls. At 45 days, radioactivity at the L4–5 lumbar regions of SOD1^{G93A} and age-matched control mice was comparable. However, at 65 days (presymptomatic stage), the SOD1^{G93A} mice revealed a 43% reduction in peak radioactivity at the L4–5 regions ($p < 0.0005$, see Table S1) without any change in the time to the peak uptake. As the disease progressed with age, the abnormality of net retrograde axonal transport worsened. By 85 days (pre- or minimally symptomatic), there was a 58% reduction in amplitude of relative peak radioactivity at the L4–5 regions, as well as a delay of approximately 20 hours in the time to the peak. Further progression was evident at late symptomatic and end stages, at which respectively there were reductions in peak radioactivity of 64% and 70%, associated with 48% and 76% delays in the time to peak (see Table S1). These studies demonstrate that in this mouse model this assay defines a quantitative, progressive defect that correlates with progressive worsening of the motor neuron disease.

Recently, we generated a transgenic mouse model expressing ALS-associated mutations in profilin-1 (*PFN1*).[26,37] Like the SOD1 model, these mice display age-dependent motor neuron loss, paralysis, and death. At 230 days, when motor function is noticeably abnormal,[26] we observed a ∼73% reduction of peak net retrograde axonal transport and subtle slowing of time to peak in the Thy1.2-PFN1$^{C71G/C71G}$ mice (Fig S1). These data demonstrate that this functional biomarker may be broadly useful in diverse categories of motor neuron disorders.

CRISPR/Cas9 Gene Targeting Ameliorates Net Retrograde Axonal Transport Deficiency in SOD1^{G93A} Mice

To determine whether net retrograde axonal transport might provide a sensitive, early indication of benefit from a therapeutic intervention in ALS, we characterized the effect of CRISPR-Cas9-mediated gene targeting of *SOD1* on the net axonal transport of the SOD1^{G93A} mice. We designed and validated an sgRNA targeting *SOD1* in vitro and generated adeno-associated viral vectors, one containing the SOD1 sgRNA and the other containing Cas9 from *Streptococcus pyogenes*. We codelivered the AAVs to the central nervous system of neonatal SOD1^{G93A} mice via intracerebroventricular injection (Fig 3, n = 39). We used 3 control groups: (1) mice codelivered AAV.Cas9 with an AAV vector expressing an sgRNA targeting the bacterial *LacZ* gene (hereafter called sgControl, n = 13), (2) mice receiving only the AAV.Cas9 vector (n = 14), and (3) an untreated group (n = 13). Delivery of AAV.Cas9 with AAV.sgSOD1 generated insertion/deletion mutations at the predicted *SOD1* locus, the most common of which was the insertion of an adenosine 4 nucleotides upstream of the Cas9's protospacer adjacent motif sequence. At 110 days, SOD1 expression was reduced in microdissected lumbar spinal motor neurons (∼50% reduction detected by gel capillary Western blotting $p > 0.05$). By contrast, levels of SOD1 protein in homogenates of whole lumbar spinal cord were not significantly reduced. At this time point, there was a corresponding reduction of SOD1 protein expression in the cortex (68% reduction in SOD1 protein as compared to sgControl mice and detected by ELISA, $p = 0.033$). These findings document that CRISPR-based editing of the *SOD1* gene attenuates expression of the SOD1 protein in the cortex and specifically in motor neurons in the spinal cord; the

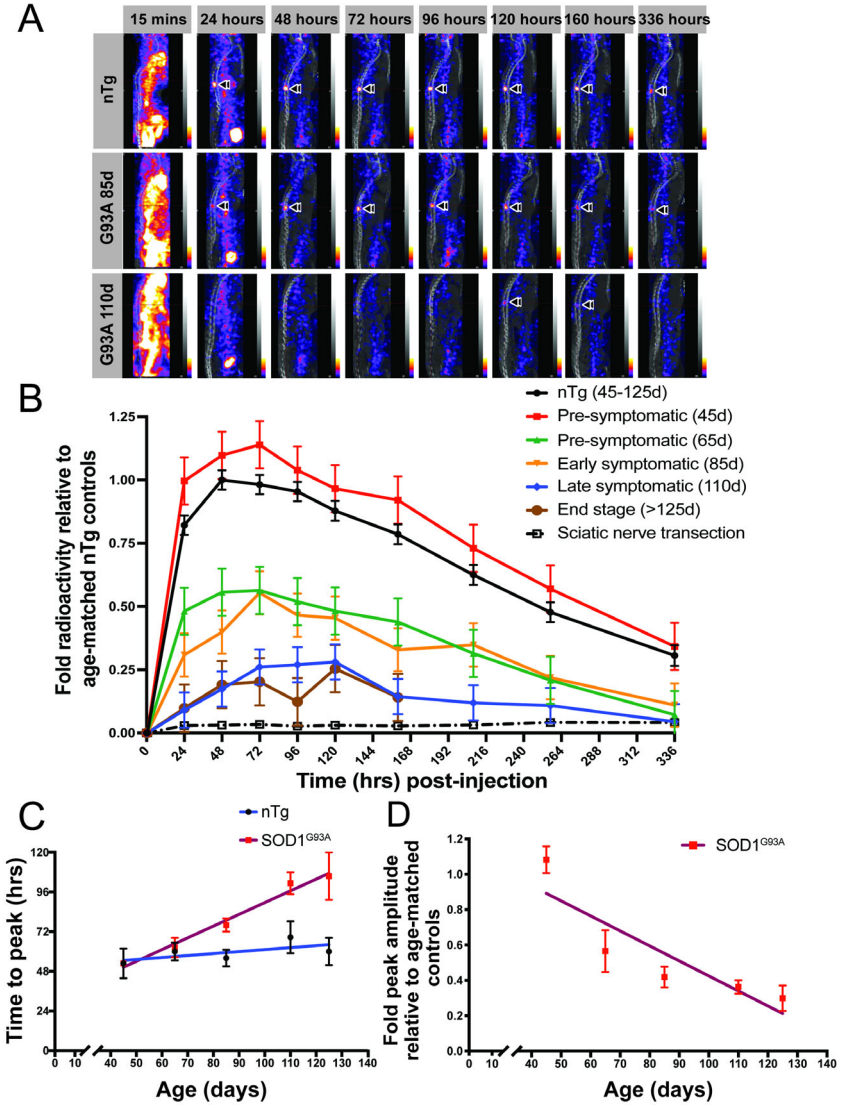

FIGURE 2: Net retrograde axonal transport is progressively impaired in mice harboring transgenes with mutant *SOD1* genes. (A) In SOD1^{G93A} transgenic and control animals, the time course of net axonal transport was determined by quantifying ^{125}I signals from single photon emission computed tomographic/computed tomographic images at the L4–5 lumbar segments as illustrated by sagittal images of mice. The top row shows an 85-day-old nontransgenic (nTg) mouse, the middle row shows a 85-day-old SOD1^{G93A} mouse, and the bottom row shows a 110-day-old SOD1^{G93A} mouse. Arrowheads point to the accumulated radiolabeled tetanus toxin fragment C (TTC) at L4–5 lumbar segments. (B) The net retrograde axonal transport becomes progressively impaired as the disease stage progresses through 4 stages: presymptomatic (45 $\pm$ 1.2 days, n = 5; 65 $\pm$ 1.2 days, n = 5), presymptomatic or minimally symptomatic (85 $\pm$ 1.3 days, n = 6), late symptomatic (110 $\pm$ 1.1 days, n = 9), and terminal stage (>125 days, n = 5). Data are presented as least-squares means relative to nTg group from time points from 24 to 336 hours based on the mixed model for repeated measures (MMRM). The overall least-squares means of net axonal transport from time point from 24 to 336 hours were compared between the nTg controls and the other groups. The least-squares mean differences (95% confidence intervals) were -0.11 ± 0.09 (-0.29 to 0.07) between the 45-day-old and nTg groups, 0.34 ± 0.09 (0.16–0.52) between the 65-day-old and nTg groups, 0.40 ± 0.08 (0.24–0.57) between the 85-day-old and wild-type groups, and 0.59 ± 0.07 (0.45–0.74) between the 110-day-old and nTg groups. Net retrograde axonal transport is significantly smaller in all the groups except the 45-day-old group than the nTg group. See Table S1 with the full MMRM analysis for *p* values. (C) The time to peak becomes prolonged with age in SOD1^{G93A} mice (red with magenta line, $R^2 = 0.98$) but not the nTg controls (black with blue line, $R^2 = 0.432$). (D) The relative amplitude of peak radioactivity declines ($R^2 = 0.783$) as the disease progresses in SOD1^{G93A} mice. Error bars represent standard error.

latter findings are consistent with earlier evidence that AAV9 vectors preferentially transfect motor neurons.[38]

At day 85, net retrograde axonal transport was fully preserved in the CRISPR-treated SOD1^{G93A} mice and distinctly better than in untreated mice (Fig 4, Video VIDEO S2, Table S1). At that time point, the mice were all asymptomatic or minimally symptomatic. This TTC-based documentation of the benefit of *SOD1* gene editing

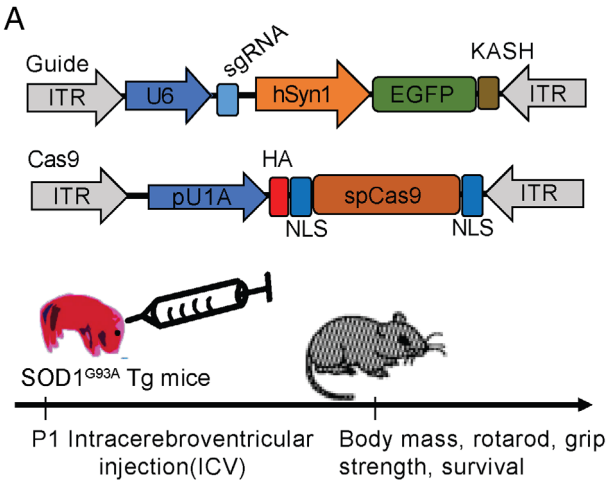

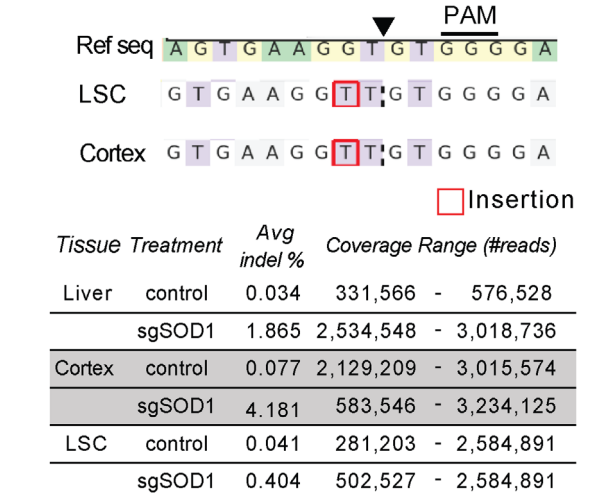

Tissue	Treatment	Avg indel %	Coverage Range (#reads)
Liver	control	0.034	331,566 - 576,528
	sgSOD1	1.865	2,534,548 - 3,018,736
Cortex	control	0.077	2,129,209 - 3,015,574
	sgSOD1	4.181	583,546 - 3,234,125
LSC	control	0.041	281,203 - 2,584,891
	sgSOD1	0.404	502,527 - 2,584,891

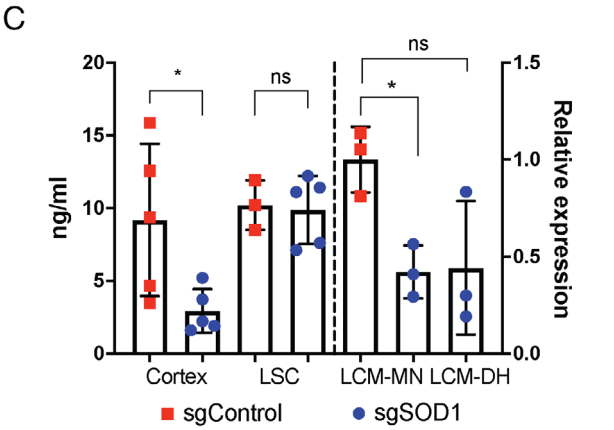

FIGURE 3: CRISPR-mediated suppression of *SOD1* in SOD1^{G93A} mice. (A) Experimental paradigm. SOD1^{G93A} neonate mouse pups (postnatal day 1) were injected via intracerebroventricular injections with dual AAV9 vectors expressing either Cas9 or sgSOD1 (n = 39). Control cohorts include mice treated with AAV9.Cas9 only (n = 14), AAV9.Cas9 + AAV9.sgControl mice (n = 13), and untreated mice (n = 13). (B) In the upper panel, representative reads from deep sequencing of the *SOD1* target region show on-target editing of *SOD1* in lumbar spinal cord and cortex. The black triangle shows the predicted cut site. The lower panel shows a table quantifying percentage reads that reveal editing, as denoted by insertion–deletions (indels) around the *SOD1* cut site. (C) SOD1 protein expression in cortex and lumbar spinal cord (LSC) of end-stage mice treated with either Cas9 + sgSOD1 or Cas9 + sgControl. The left side of the histogram shows the enzyme-linked immunosorbent assay data for homogenates of cortex (n = 5 for both sgSOD1 or sgControl) and lumbosacral cord (sgSOD1 n = 5, sgControl n = 3; Student *t* test, *$p < 0.05$). The right side of the histogram illustrates the relative expression of SOD1 protein/total protein as quantified using gel capillary Western blotting for laser-captured motor neurons (LCM-MN) or residual dorsal horn (LCM-DH) tissue from 100-day-old Cas9 + sgSOD1 compared to Cas9 + sgControl mice (n = 150 neurons in each group from 3 independent experiments, Student *t* test, *$p < 0.05$). Error bars represent standard deviation. ANC1, SYNE homology; EGFP = enhanced green fluorescent protein; HA = hemagglutinin; ITR = inverted terminal repeat; KASH = Klarsicht, NLS = nuclear localization sequence; ns = not significant; PAM = protospacer adjacent motif; Tg = transgenic. U6 and pU1A are the promoters for the indicated constructs.

(Figure legend continues on next column.)

was evident well before standard behavioral tests distinguished treated from untreated mice (eg, by grip strength at ~100 days and rotarod at ~120 days. Compared to control mice that received Cas9 and a nontargeting control, sgSOD1-treated mice exhibited increased survival (median survival = 154 vs 134 days of sgControl + Cas9, $p < 0.0001$), improved ventral root counts, and preservation of neuromuscular junction integrity. These data show that net retrograde axonal transport demonstrates early and distinct benefit from a therapeutic intervention in clinically normal ALS mice, well in advance of behavioral or survival parameters.

Net Retrograde Axonal Transport Is Impaired in C9ORF72 Transgenic Mice

A useful attribute of a biomarker for the integrity of the motor unit is the ability to detect perturbations in function that are biologically important but too subtle to be reflected in clinical manifestations. We have therefore used the uptake of ^{125}I-TTC to L4–5 motor neurons to study a line of mice that harbor a human transgene with the ALS-associated *C9ORF72* gene with ~600 copies of the GGGGCC intronic repeat.[27] Although these C9BAC animals do not recapitulate the motor phenotypes of ALS, they have disease-specific histopathological features including intranuclear RNA foci and poly(glycine-proline) dipeptides. We administered ^{125}I-TTC into the gastrocnemius muscle of 24-month-old C9BAC transgenic mice and age-matched nontransgenic controls and followed uptake at L4–5 by SPECT/CT imaging at 24-hour or 48-hour intervals for 2 weeks. Whereas the time profile of uptake, including time to peak uptake, was equivalent

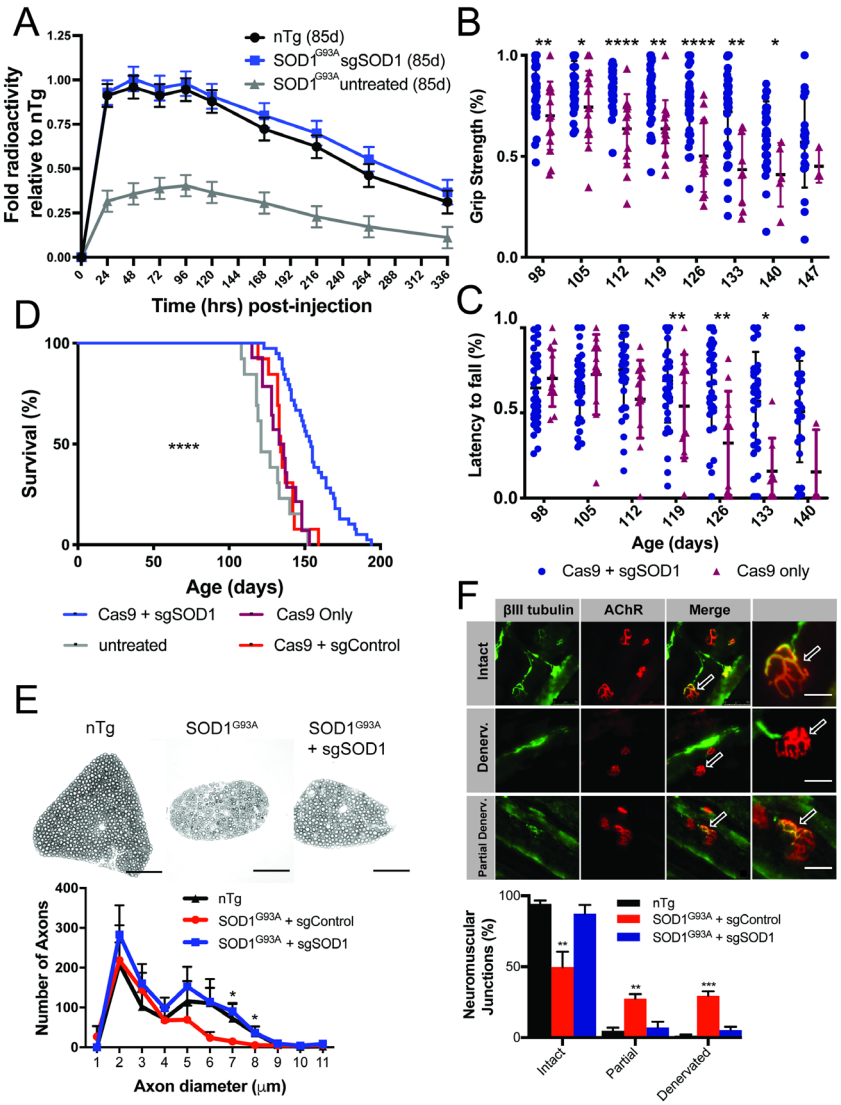

FIGURE 4: Net retrograde axonal transport detects early improvement after CRISPR-mediated knockdown of *SOD1*. (A) Improvement in net retrograde axonal transport of 85-day-old SOD1^{G93A} mice after gene editing. Black indicates net transport in wild-type nontransgenic (nTg) mice (n = 6). Gray indicates untreated SOD1^{G93A} mice (Cas9 + sgControl mice, n = 8). Blue indicates treated SOD1^{G93A} mice (Cas9 + sgSOD1, n = 7). Data are presented as least-squares means relative to nTg group from time points from 24 to 336 hours based on the mixed model for repeated measures (MMRM). The overall least-squares means of net axonal transport from time points from 24 to 336 hours were compared between the nTg group and the other group. The least-squares mean differences (95% confidence intervals) were 0.05 ± 0.09 (−0.13 to 0.24) with a *p* value of 0.57 between the nTg control and the treated SOD1^{G93A} groups, and 0.45 ± 0.09 (0.27–0.63) between the nTg group and the untreated SOD1^{G93A} group. Net retrograde axonal transport is significantly lower in the untreated mice than the treated mice, with a *p* value of <0.0001 using the MMRM (see Table S1). (B) Grip-strength recordings and (C) rotarod measurements of sgSOD1 mice (n = 38) versus control mice treated with Cas9 only (n = 14; Student *t* test, **p* < 0.05, ***p* < 0.01, *****p* = 0.0001). Error bars represent standard deviation (SD). (D) Kaplan–Meier curve representing lifespan showing significant difference in survival of Cas9 + sgSOD1 compared to Cas9 + sgControl mice (Cas9 + sgSOD1, n = 38; Cas9 + sgControl, n = 13; Cas9 only, n = 14; untreated, n = 13; log-rank test, *****p* < 0.0001). (E) Quantitative ventral root analysis at disease midpoint (day 110) comparing wild-type to sgSOD1 and sgControl mice (n = 3 per group). Top: Representative images of ventral roots from nTg, sgSOD1, and sgControl mice. Scale bars = 100μm. Bottom: Ventral root counts grouped by axon diameter. The numbers of large diameter axons (>4μm, corresponding to motor neuron axons) are decreased in SOD1^{G93A} sgControl mice as compared to SOD1^{G93A} sgSOD1 and nTg mice (Student *t* test, **p* < 0.05). This preferential loss of large alpha motor neurons with relative sparing of the gamma motor neurons is a documented feature of the transgenic SOD1^{G93A} amyotrophic lateral sclerosis mice.[39,40] (F) Status of the neuromuscular junctions (NMJs) at disease midpoint (day 110) in gastrocnemius muscle from nTg (n = 3), sgSOD1 (n = 3), or sgControl mice (n = 3). Top: Representative images showing intact, partially denervated, and fully denervated neuromuscular junctions. Bar = 50μm. Bottom: relative to nTg mice, sgSOD1 mice had 87.3% intact NMJs compared to 49.7% of sgControl. Conversely, sgSOD1 mice had 7.3% partially denervated NMJs (compared to sgControl, 27.4%), and 5.3% fully denervated NMJs (compared to sgControl, 29.6%; Student *t* test, ***p* < 0.01, ****p* < 0.001). Error bars denote SD. AChR = acetylcholine receptor.

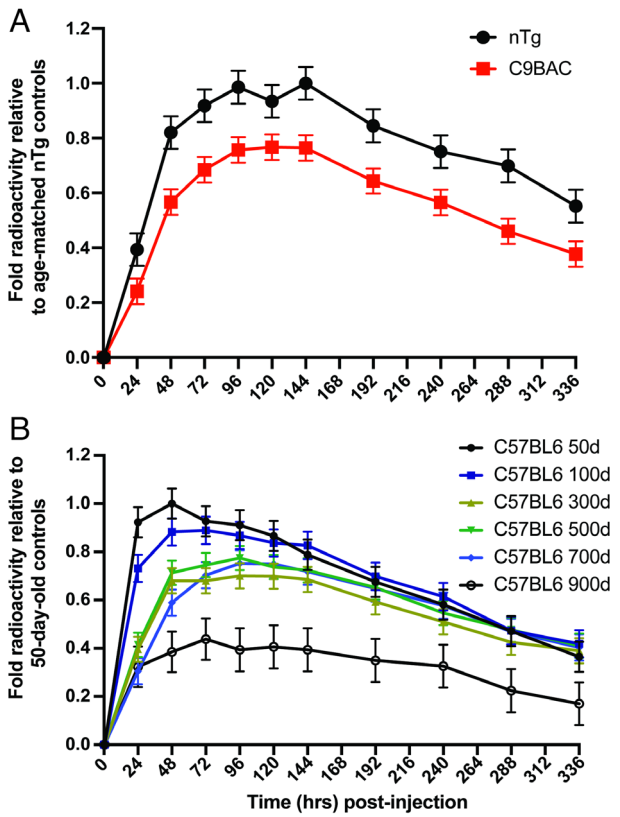

FIGURE 5: Net retrograde axonal transport in transgenic *C9ORF72* mice and in aging mice. (A) Net retrograde axonal transport in 24-month-old C9BAC transgenic mice (n = 10, red lines) and the corresponding nontransgenic (nTg) littermates (n = 10, *black lines*) are illustrated. Data are presented as least-squares means relative to nTg group from time points from 24 to 336 hours based on the mixed model for repeated measures (MMRM). The overall least-squares means of net axonal transport from time points from 24 to 336 hours were compared between the nTg and the C9BAC groups. The least-squares mean differences (95% confidence intervals) were 0.21 (0.07–0.35) between the two groups. Net retrograde axonal transport is significantly smaller in the C9BAC group than the nTg group, with a *p* value of 0.0071 (see Table S1). (B) Net retrograde axonal transport of C57BL6 mice is illustrated at 6 different ages: 50 (n = 9), 100 (n = 11), 300 (n = 13), 500 (n = 14), 700 (n = 12), and 900 days (n = 5). Data are presented as least-squares means relative to the 50-day-old group from time points from 24 to 336 hours based on the MMRM. The overall least-squares means of net axonal transport of C57BL6 mice from time points from 24 to 336 hours were compared between the young 50-day-old (50d) group and the other groups. The least-squares mean differences (95% confidence intervals) were 0.03 ± 0.08 (−0.13 to 0.19) between the 50- and 100-day-old groups, 0.17 ± 0.08 (0.02–0.33) between the 50- and 300-day-old groups, 0.13 ± 0.08 (0.02–0.28) between the 50- and 500-day-old groups, 0.16 ± 0.08 (0.004–0.32) between the 50- and the 700-day-old groups, and 0.41 ± 0.1 (0.21–0.61) between the 50- and the 900-day-old groups. Net retrograde axonal transport is significantly smaller in the very old group than the young and healthy groups, with a *p* value of 0.0001 (see Table S1).

postinjection in both cohorts, the peak uptake of ^{125}I-TTC was significantly lower (∼22% reduction) in the C9BAC mice (Fig 5A, p < 0.007, Table S1). Additionally, we obtained from collaborators an independent line of younger (15-month-old) transgenic mice carrying the same C9BAC construct. In these mice, the profile of net ^{125}I-TTC transport was identical to that in our mice. These data further encourage the view that net retrograde axonal transport of TTC is promising as a biomarker for detection of subclinical motor neuron pathology.

Net Retrograde Axonal Transport Is Mildly Delayed in Aging Animals

Although many age-dependent physiological changes compromise viability of neurons, the impact of aging on axonal transport has not been evaluated in detail. We therefore sought to quantify net retrograde axonal transport in cohorts of wild-type mice at different ages. Following its injection into the gastrocnemius muscle, we quantified ^{125}I-TTC uptake in the L4–5 region in 50-, 100-, 300-, 500-, 700-, and 900-day-old C57BL6 mice. Peak uptake was greatest, and the time to peak the most rapid, in the 50- and 100-day-old animals (see Fig 5B). By comparison, in the 300-, 500-, 700-, and 900-day-old animals, there was a statistically significant fall-off in both parameters over time.

Immunization Reduces but Does Not Eliminate Net Retrograde Axonal Transport of ^{125}I-TTC

This technique of visualizing net retrograde axonal transport has broad application in human motor neuron disorders. An important consideration is that most individuals in North America and Europe have been immunized with TT. We therefore sought to investigate the impact of immunization of TT on the analysis of TTC uptake. We administered wild-type mice 2 consecutive immunizations of TT or PBS at 8 and then 14 weeks of age. We then assayed the net axonal transport of ^{125}I-TTC at 20 weeks of age (12 weeks from the initial immunization; red profile in Fig 6). After immunization with TT, the mice developed antibody titers against TT as expected. Mice immunized with TT demonstrated ^{125}I-TTC uptake with a time profile identical to that of nonimmunized controls but with a reduced total amplitude of uptake (approximately 45% reduction) as compared to nonimmunized controls. One possible application of our transport assay is to determine how transport is affected by a trial compound, comparing net transport at baseline and after starting a trial therapy. We therefore asked whether repeat administrations of TTC will further attenuate the peak amplitude of net retrograde axonal transport. To test this, we conducted a second net axonal transport assay on these immunized mice 10 weeks after the initial assay (22 weeks after the initial immunization, green profile in Fig 6B, Table S1). This second transport assay was not associated

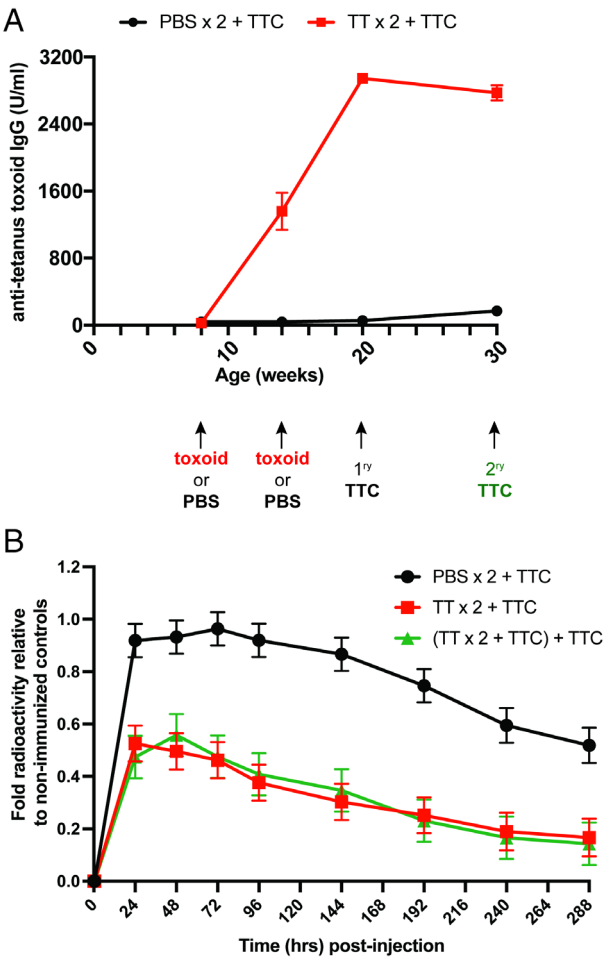

FIGURE 6: Immunization with tetanus toxoid (TT) and tetanus toxin fragment C (TTC) reduces but does not eliminate net retrograde axonal transport. (A) The titer of anti-TT antibodies is illustrated for the key time points in the experiment. Two cohorts of age-matched C57BL6 mice (n = 12 for each group) received two consecutive injections of either TT or phosphate-buffered saline (PBS), first at 8 weeks of age and subsequently at 14 weeks. Twelve weeks after the primary vaccination (at age 20 weeks), both groups received ^{125}I-TTC to characterize net retrograde axonal transport. Ten weeks later (at age 30 weeks), a repeat net axonal transport assay was performed on the previously immunized animals along with a new control set of naïve nonimmunized controls (n = 4). The antibody titers against TT in mice that received a primary and booster shots of TT were significantly elevated ($p < 0.0001$; repeated measures two-way analysis of variance after Bonferroni correction as compared to the mice with PBS treatments). (B) The resulting net retrograde axonal transport profile is illustrated for mice that received two toxoid injections (red; n = 10) or PBS (black; n = 13). Data from mice immunized twice with TT then TTC, whose TTC transport was reassayed at age 30 weeks, are in green (n = 8). For mice receiving two TT immunizations and either one or two TTC injections, the reduction in transport as compared to wild-type mice is significant ($p < 0.0001$, see Table S1); the overall least-squares mean differences ± standard error (95% confidence interval) was 0.46 ± 0.08 (0.28–0.63). However, those two groups had essentially the same net retrograde axonal transport profile as compared to the control group *(Figure legend continues on next column.)*

with a further reduction of the net axonal transport. This indicates that immunization of TT partially blocks the net retrograde axonal transport of TTC, but that it remains feasible subsequently to use TTC transport as a biomarker for efficacy of therapies in disorders like ALS.

Discussion

This report describes a novel method to quantify the net retrograde axonal transport of TTC from muscle to the spinal cord. A previous report described a fluorescence-based, noninvasive method to detect TTC uptake into the spinal cord in mice but, by contrast with the present approach, did not permit quantification of uptake within specific segments of the spinal cord, was not used repeatedly in the same mice, and was not tested as a disease or therapeutic biomarker.[41] Our assay exploits the binding of TTC to ganglioside GT_{1b} at the presynaptic terminal at the NMJ followed by axonal transport in clathrin-dependent endocytic pathway toward the cell body. After transport to motor neurons, TTC is trans-synaptically released from the motor neurons to the surrounding neuropil and presynaptic structures.[42] Our immunostaining study illustrates that TTC is taken up by the GAD67^{+}-GABAergic interneurons (see Fig 1D). Surprisingly, as gauged by our imaging studies, the trans-synaptically released TTC that is subsequently taken up by interneurons has a slow turnover cycle and is only minimally cleared from the anterior horn. This property permits serial visualization and quantification of TTC accumulation in the ventral horn of the spinal cord for prolonged periods (eg, 336 hours or two weeks in Fig 1C).

We have focused on two parameters in describing net retrograde axonal transport: the amplitude of peak uptake (normalized to controls) and the time to peak uptake. These reflect several factors, primarily including the total number of viable motor neurons, the rate of retrograde axonal transport, and the integrity of NMJs. At least in theory, transport may also be influenced non-cell autonomously by other cells, including microglia, interneurons, and astroglia. In SOD1^{G93A} transgenic animals, for example, we observed a substantial decrease in relative peak amplitude values in presymptomatic animals

($p = 0.968$), with the least-square mean differences ± standard error (95% confidence interval) being 0.004 ± 0.096 (−0.19 to 0.2). In panel A, the group that received two PBS treatments followed by the ^{125}I-TTC assay is designated as "PBS × 2 + TTC" (black). The group that received two TT treatments followed by the ^{125}I-TTC assay is designated as "TT × 2 + TTC" (red). Panel B also depicts the third group that underwent a follow-up ^{125}I-TTC transport assay; this group is designated as "(TT × 2 + TTC) + TTC" (green).

(65 days old), whereas this decrease was absent 20 days earlier (45 days old; see Fig 2A). This corresponds well with the documented axonopathy that entails denervation of fast-fatigable motor neurons at 55 days.[43–45] Minimally symptomatic animals at 85 days of age demonstrated a reduction of peak amplitude comparable to the early symptomatic animals but additionally showed a 17% delay of time to peak. This slight delay of time-to-peak value may reflect the combined impacts of denervation and subsequent reinnervation by more resistant motor neurons; it corresponds well with the finding that reinnervation of fast-fatigable NMJs by fast-fatigue-resistant motor neurons occurs at day 70.[43] By the late symptomatic and terminal stages (110 and >125 days, respectively), we observed a further reduction of relative peak amplitude and a longer time-to-peak value. These findings are consistent with previous reports that there is denervation of fast-fatigue-resistant motor neurons by 50 days[43,44] and fractional loss of all motor neurons of 40 and 56% at 95 and 113 days, respectively.[9]

Numerous studies have demonstrated that repressing expression of mutant *SOD1* in $SOD1^{G93A}$ transgenic mice delays onset and increases survival.[29,46] Our strategy of using CRISPR-Cas9 to suppress *SOD1* using dual AAV9 viral vectors produced a robust clinical improvement of net retrograde axonal transport as early as day 85, at which time the mice are clinically normal, with the exception of a few mice that had leg tremors. At this time point, the peak transport amplitudes were normal in treated mice, whereas untreated transgenic mice had a 60% reduction in relative peak amplitude. Thus, at 85 days, the net retrograde axonal transport assay documented the efficacy of *SOD1* editing well before standard behavioral assays; the difference between untreated and treated mice was not evident by weight analysis and grip strength until ~100 days or by rotarod until ~120 days.

Deep sequencing of the *SOD1* locus revealed relatively low levels of genetic editing of *SOD1* (~4% in brain and 0.4% in spinal cord), yet this sufficed to repress *SOD1* expression and improve the disease course. This observation matches a comparable finding in an earlier study of CRISPR-Cas9 targeting *SOD1*[47] in which editing of *SOD1* was estimated to be ~0.2 to 0.4% in the spinal cord. In our study, we demonstrate a larger reduction in SOD1 protein levels, specifically in motor neurons after laser capture (see Fig 3C); this may account for the significant effect on survival compared to the small effect on genetic editing. Furthermore, deep sequencing of the *SOD1* locus may not report large scale deletions, which would underestimate the actual editing rate.[48]

Noncoding expansions of the GGGGCC hexanucleotide repeat in the *C9ORF72* gene represent the most common mutation in familial ALS/frontotemporal dementia. Our *C9ORF72* transgenic mice exhibited histopathological hallmarks of RNA foci and dipeptide protein formation without behavioral and electrophysiological abnormalities or denervation of NMJs.[27] We characterized the net retrograde TTC transport in 700-day-old *C9ORF72* transgenic mice and their age-matched controls. Whereas the transport dynamics of these two groups share comparable temporal profiles (time-to-peak values ranging 120–144 hours, see Fig 5A), the relative peak-amplitude value in the transgenic animals revealed a significant reduction compared to the controls. These data argue that some component of net retrograde axonal transport in the *C9ORF72* transgenic mice is compromised. We know that it is neither denervation nor loss of motor neurons, suggesting instead that the amplitude loss reflects defects in actual axonal transport, or in some other property of the *C9ORF72* transgenic motor unit. Most importantly, this subtle yet significant disturbance of net retrograde axonal transport demonstrates the sensitivity of our method, which detected transport deficiencies even in the absence of an overt clinical phenotype. It is conceivable that this or similar assays, which detect otherwise inapparent motor unit pathology, may illuminate perplexing and sometimes disabling disorders for which conventional clinical studies have been uninformative (eg, chronic fatigue syndrome).

In wild-type C57BL6 mice, we detected subtle alterations of net retrograde axonal transport deficits with age. In the 900-day-old animals, there was a significant decrease in the relative peak-amplitude. Additionally, there was an age-dependent slowing in the time-to-peak values between younger animals (50- and 100-day-old animals) and older animals (300, 500, 700, and 900 days old). These findings likely reflect both NMJ denervation[49-51] and some impact of aging on transport itself. As in the *C9ORF72* transgenic mice above, these findings underscore the sensitivity of this method to define alterations in net retrograde axonal transport in the absence of overt weakness.

Retrograde TTC transport permits repetitive quantitative assessment of the status of motor units in living mammals. However, a potential hurdle to consider in moving this to the clinic is the presence of neutralizing antibodies in the sera of most individuals in North America and Europe, a consequence of widespread tetanus vaccination. To ascertain whether tetanus vaccination affects retrograde uptake of TTC, Fishman et al quantified transported rhodamine-labeled TTC in the hypoglossal with TT.[52] Despite elevated titers of antibody against TTC in the vaccinated animals, the net uptake of TTC in the hypoglossal nucleus was readily detected and not reduced

by vaccination. Similarly, in our study, TTC uptake was also readily detected after TT vaccination (with an approximate 50% reduction in the TTC uptake profile, see Fig 6B). In our mice, although the TT immunization partially attenuated the net axonal uptake of TTC, we did not see a further reduction of TTC delivery when we repeated the net axonal transport assay 10 weeks later. This validates the clinical potential of our technique; it is evident that immunization generated through two TTC administrations will not mask the net retrograde axonal transport profile. This is important in a clinical setting, wherein it is important to repeat the net retrograde axonal transport assay in the same patient to monitor the impact of a potential therapy.

The novel, noninvasive method reported here to quantify net retrograde TTC transport in vivo has several characteristics of a valuable biomarker. It can be used repeatedly in the same subject over time and permits detection of clinical and subclinical abnormalities in disease and normal aging. It is informative in diverse mouse models and across a wide range of physiological states in the motor unit. Perhaps most importantly, it permits early detection of benefit from potential therapies in motor neuron disease. Although these proof-of-concept experiments were conducted in mice, we believe that this assay will potentially have broad clinical utility for human motor neuron diseases (presumably with a shorter half-life isotope label such as ^{123}I-iodine or ^{111}indium).

Acknowledgments

We acknowledge support from the NIH National Institute of Neurological Disorders and Stroke (5R01NS101895 to Z.X.; UL1-TR001453 and RO1-NS088689 to R.H.B.), and from ALS Finding a Cure, the Angel Fund for ALS Research, ALSOne, Project ALS, the Max Rosenfeld Fund for ALS Research, and Target ALS.

We thank Dr P. Fishman (University of Maryland) for providing N18-RE-105 cell line, Dr C. Baer and the Sanderson Center for Optical Experimentation (UMass Chan Medical School) for providing the slide scanning services, Dr F. Zhang for providing plasmid hSyn-GFP-KASH-bGH, and Drs M. S. Klempner, F. Fazio, and P. Bergonzi (MassBiologics, UMass Chan Medical School) for providing purified TT. We are also grateful for the technical assistance of J. Francis, N. Wightman, R. Chian, A. Weiss, J. Metterville, and O. Peters from the Brown laboratory, and H. Mou and S. Kwan from the Xue laboratory; and for the helpful comments of Drs. N. Aronin, D. Bosco, V. Budnik, R. Davis, M. Freeman, M. Garber, L. Hayward, O. King, and D. Schafer from the University of Massachusetts Medical School.

Author Contributions

R.H.B., P.-T.J.L., Z.K., M.R., and W.X. contributed to the conception and design of the study. R.H.B., P.-T.J.L., Z.K., Y.W., Y.L., C.C. O.U., B.M.d.C.G., Z.X., and M.R. contributed to the acquisition and analysis of data. R.H.B., P.-T.J.L., Z.K., Y.L., C.C., C.-Q.S, Z.X., and M.R. contributed to drafting the text and or preparing the figures.

Potential Conflicts of Interest

Nothing to report.

References

1. Adalbert R, Coleman MP. Review: axon pathology in age-related neurodegenerative disorders. Neuropathol Appl Neurobiol 2013;39:90–108.
2. Breuer AC, Lynn MP, Atkinson MB, et al. Fast axonal transport in amyotrophic lateral sclerosis: an intra-axonal organelle traffic analysis. Neurology 1987;37:738–748.
3. Sasaki S, Iwata M. Impairment of fast axonal transport in the proximal axons of anterior horn neurons in amyotrophic lateral sclerosis. Neurology 1996;47:535–540.
4. Zhang B, Tu P, Abtahian F, et al. Neurofilaments and orthograde transport are reduced in ventral root axons of transgenic mice that express human SOD1 with a G93A mutation. J Cell Biol 1997;139:1307–1315.
5. Warita H, Itoyama Y, Abe K. Selective impairment of fast anterograde axonal transport in the peripheral nerves of asymptomatic transgenic mice with a G93A mutant SOD1 gene. Brain Res 1999;819:120–131.
6. Williamson T, Cleveland D. Slowing of axonal transport is a very early event in the toxicity of ALS-linked SOD1 mutant to motor neurons. Nat Neurosci 1999;1:50–56.
7. Ligon LA, LaMonte BH, Wallace KE, et al. Mutant superoxide dismutase disrupts cytoplasmic dynein in motor neurons. Neuroreport 2005;16:533–536.
8. Bosco DA, Morfini G, Karabacak NM, et al. Wild-type and mutant SOD1 share an aberrant conformation and a common pathogenic pathway in ALS. Nat Neurosci 2010;13:1396–1403.
9. Bilsland LG, Sahai E, Kelly G, et al. Deficits in axonal transport precede ALS symptoms in vivo. Proc Natl Acad Sci U S A 2010;107:20523–20528.
10. Magrane J, Sahawneh MA, Przedborski S, et al. Mitochondrial dynamics and bioenergetic dysfunction is associated with synaptic alterations in mutant SOD1 motor neurons. J Neurosci 2012;32:229–242.
11. Magrane J, Cortez C, Gan WB, Manfredi G. Abnormal mitochondrial transport and morphology are common pathological denominators in SOD1 and TDP43 ALS mouse models. Hum Mol Genet 2014;23:1413–1424.
12. Morfini GA, Bosco DA, Brown H, et al. Inhibition of fast axonal transport by pathogenic SOD1 involves activation of p38 MAP kinase. PLoS One 2013;8:e65235.

13. Wang W, Li L, Lin WL, et al. The ALS disease-associated mutant TDP-43 impairs mitochondrial dynamics and function in motor neurons. Hum Mol Genet 2013;22:4706–4719.

14. Alami NH, Smith RB, Carrasco MA, et al. Axonal transport of TDP-43 mRNA granules is impaired by ALS-causing mutations. Neuron 2014; 81:536–543.

15. Clark JA, Southam KA, Blizzard CA, et al. Axonal degeneration, distal collateral branching and neuromuscular junction architecture alterations occur prior to symptom onset in the SOD1(G93A) mouse model of amyotrophic lateral sclerosis. J Chem Neuroanat 2016;76: 35–47.

16. Landers JE, Melki J, Meininger V, et al. Reduced expression of the kinesin-associated protein 3 (KIFAP3) gene increases survival in sporadic amyotrophic lateral sclerosis. Proc Natl Acad Sci U S A 2009; 106:9004–9009.

17. Wu CH, Fallini C, Ticozzi N, et al. Mutations in the profilin 1 gene cause familial amyotrophic lateral sclerosis. Nature 2012;488: 499–503.

18. Kenna KP, van Doormaal PT, Dekker AM, et al. NEK1 variants confer susceptibility to amyotrophic lateral sclerosis. Nat Genet 2016;48: 1037–1042.

19. Smith BN, Ticozzi N, Fallini C, et al. Exome-wide rare variant analysis identifies TUBA4A mutations associated with familial ALS. Neuron 2014;84:324–331.

20. Zhang F, Strom AL, Fukada K, et al. Interaction between familial amyotrophic lateral sclerosis (ALS)-linked SOD1 mutants and the dynein complex. J Biol Chem 2007;282:16691–16699.

21. Strom AL, Shi P, Zhang F, et al. Interaction of amyotrophic lateral sclerosis (ALS)-related mutant copper-zinc superoxide dismutase with the dynein-dynactin complex contributes to inclusion formation. J Biol Chem 2008;283:22795–22805.

22. Taylor JP, Brown RH Jr, Cleveland DW. Decoding ALS: from genes to mechanism. Nature 2016;539:197–206.

23. Altman T, Ionescu A, Ibraheem A, et al. Axonal TDP-43 condensates drive neuromuscular junction disruption through inhibition of local synthesis of nuclear encoded mitochondrial proteins. Nat Commun 2021;12:6914.

24. Benn SC, Ay I, Bastia E, et al. Tetanus toxin fragment C fusion facilitates protein delivery to CNS neurons from cerebrospinal fluid in mice. J Neurochem 2005;95:1118–1131.

25. Rogers TB, Snyder SH. High affinity binding of tetanus toxin to mammalian cell membranes. J Biol Chem 1981;256:2402–2407.

26. Yang C, Danielson EW, Qiao T, et al. Mutant PFN1 causes ALS phenotypes and progressive motor neuron degeneration in mice by a gain of toxicity. Proc Natl Acad Sci U S A 2016;113:E6209–E6218.

27. Peters OM, Cabrera GT, Tran H, et al. Human C9ORF72 hexanucleotide expansion reproduces RNA foci and dipeptide repeat proteins but not neurodegeneration in BAC transgenic mice. Neuron 2015;88:902–909.

28. Platt RJ, Chen S, Zhou Y, et al. CRISPR-Cas9 knockin mice for genome editing and cancer modeling. Cell 2014;159:440–455.

29. Stoica L, Todeasa SH, Toro Cabrera G, et al. AAV delivered artificial microRNA extends survival and delays paralysis in an amyotrophic lateral sclerosis mouse model. Ann Neurol 2016;79:687–700.

30. Borel F, Gernoux G, Sun H, et al. Safe and effective superoxide dismutase 1 silencing using artificial microRNA in macaques. Sci Transl Med 2018;10:eaau6414.

31. Staub GC, Walton KM, Schnaar RL, et al. Characterization of the binding and internalization of tetanus toxin in a neuroblastoma hybrid cell line. J Neurosci 1986;6:1443–1451.

32. MacKenzie CR, Hirama T, Lee KK, et al. Quantitative analysis of bacterial toxin affinity and specificity for glycolipid receptors by surface plasmon resonance. J Biol Chem 1997;272:5533–5538.

33. Meckler RL, Baron R, McLachlan EM. Selective uptake of C-fragment of tetanus toxin by sympathetic preganglionic nerve terminals. Neuroscience 1990;36:823–829.

34. Hughes DI, Scott DT, Todd AJ, Riddell JS. Lack of evidence for sprouting of Abeta afferents into the superficial laminas of the spinal cord dorsal horn after nerve section. J Neurosci 2003;23:9491–9499.

35. Herreros J, Lalli G, Schiavo G. C-terminal half of tetanus toxin fragment C is sufficient for neuronal binding and interaction with a putative protein receptor. Biochem J 2000;347:199–204.

36. Perreault MC, Pastor-Bernier A, Renaud JS, et al. C fragment of tetanus toxin hybrid proteins evaluated for muscle-specific transsynaptic mapping of spinal motor circuitry in the newborn mouse. Neuroscience 2006;141:803–816.

37. Fil D, DeLoach A, Yadav S, et al. Mutant profilin1 transgenic mice recapitulate cardinal features of motor neuron disease. Hum Mol Genet 2017;26:686–701.

38. Foust KD, Nurre E, Montgomery CL, et al. Intravascular AAV9 preferentially targets neonatal neurons and adult astrocytes. Nat Biotechnol 2009;27:59–65.

39. Sharma A, Lyashchenko AK, Lu L, et al. ALS-associated mutant FUS induces selective motor neuron degeneration through toxic gain of function. Nat Commun 2016;7:10465.

40. Kanning KC, Kaplan A, Henderson CE. Motor neuron diversity in development and disease. Annu Rev Neurosci 2010;33:409–440.

41. Schellingerhout D, Le Roux LG, Bredow S, Gelovani JG. Fluorescence imaging of fast retrograde axonal transport in living animals. Mol Imaging 2009;8:319–329.

42. Fishman PS, Carrigan DR. Retrograde transneuronal transfer of the C-fragment of tetanus toxin. Brain Res 1987;406:275–279.

43. Pun S, Santos AF, Saxena S, et al. Selective vulnerability and pruning of phasic motoneuron axons in motoneuron disease alleviated by CNTF. Nat Neurosci 2006;9:408–419.

44. Hegedus J, Putman CT, Gordon T. Time course of preferential motor unit loss in the SOD1 G93A mouse model of amyotrophic lateral sclerosis. Neurobiol Dis 2007;28:154–164.

45. Martin LJ, Liu Z, Chen K, et al. Motor neuron degeneration in amyotrophic lateral sclerosis mutant superoxide dismutase-1 transgenic mice: mechanisms of mitochondriopathy and cell death. J Comp Neurol 2007;500:20–46.

46. Thomsen GM, Gowing G, Latter J, et al. Delayed disease onset and extended survival in the SOD1G93A rat model of amyotrophic lateral sclerosis after suppression of mutant SOD1 in the motor cortex. J Neurosci 2014;34:15587–15600.

47. Gaj T, Ojala DS, Ekman FK, et al. In vivo genome editing improves motor function and extends survival in a mouse model of ALS. Sci Adv 2017;3:eaar3952.

48. Kosicki M, Tomberg K, Bradley A. Repair of double-strand breaks induced by CRISPR-Cas9 leads to large deletions and complex rearrangements. Nat Biotechnol 2018;36:765–771.

49. Valdez G, Tapia JC, Kang H, et al. Attenuation of age-related changes in mouse neuromuscular synapses by caloric restriction and exercise. Proc Natl Acad Sci U S A 2010;107:14863–14868.

50. Li Y, Lee Y, Thompson WJ. Changes in aging mouse neuromuscular junctions are explained by degeneration and regeneration of muscle fiber segments at the synapse. J Neurosci 2011;31:14910–14919.

51. Valdez G, Tapia JC, Lichtman JW, et al. Shared resistance to aging and ALS in neuromuscular junctions of specific muscles. PLoS One 2012;7:e34640.

52. Fishman PS, Matthews CC, Parks DA, et al. Immunization does not interfere with uptake and transport by motor neurons of the binding fragment of tetanus toxin. J Neurosci Res 2006;83:1540–1543.